Dalton Transactions

The corrosion behavior of borosilicate glass in the presence of cementitious waste forms

Journal:	*Dalton Transactions*
Manuscript ID	DT-ART-03-2024-000855.R2
Article Type:	Paper
Date Submitted by the Author:	19-Jun-2024
Complete List of Authors:	Katsenovich, Yelena; Florida International University, Applied Research Center Drozd, Vadym; Florida International University, Applied Research Center Kandel, Shambhu; Florida International University, Applied Research Center Lagos, Leonel; Florida International University, Applied Research Center Asmussen, Matthew; Pacific Northwest National Laboratory

The data supporting this article have been included as part of the Supplementary Information.

The corrosion behavior of borosilicate glass in the presence of cementitious waste forms

Yelena Katsenovich[a*], Vadym Drozd[a], Shambhu Kandel[a], Leonel Lagos[a], R. Matthew Asmussen[b*].

[a]Applied Research Center, Florida International University, 10555 W Flagler St, Miami, FL 33174

[b]Pacific Northwest National Laboratory, 902 Battelle Blvd, Richland, WA 99354

[*]Corresponding authors – Matthew Asmussen matthew.asmussen@pnnl.gov, Yelena Katsenovich katsenov@fiu.edu.

Abstract

Borosilicate glasses are widely used for radioactive waste disposal due to their ability to incorporate a variety of contaminants and radionuclides while exhibiting high durability in various disposal scenarios. This research evaluated the dissolution of borosilicate glass using both single-pass-flow-through (ASTM C1662-18) and product consistency test (ASTM C1285-21) methods with different solutions, including a cementitious-contacted water (called grout-contacted, GC, from this point) and solutions with varying levels of dissolved cementitious species such as Si, Ca, Al. The results indicated that the presence of Ca plays a crucial role in suppressing glass corrosion, as evidenced by the slower normalized dissolution rates, which were one order of magnitude lower for boron and two orders of magnitude lower for rhenium, observed in both Ca- amended and GC solutions compared to the pH 12 buffer solution. This effect is attributed to the formation of a dense, low-porosity, and strongly bonded calcium silicate hydrate (CSH) layer on the glass surface, which implies that a glass corrosion process is influenced by ion exchange involving alkalis ions Na^+, K^+, Ca^{2+}, and hydrogen-containing species.

A small number of glass particles treated in the GC solution showed minor corrosion pits in the form of shallow craters with an average diameter of approximately 500 µm. This observation is correlated with a significant reduction, 2,000 to 3,000 times lower, in the cumulative volume of glass pores, indicating that smaller pore voids were "sealed" in the presence of Ca^{2+} ions, likely attributed to the formation of CSH precipitation or other corrosion products such as calcium carbonate saturated from the grout solution. These findings suggest that the presence of dissolved Ca in the GC solution can slow down the dissolution of borosilicate glass, contrary to the expected

trend of higher dissolution rates resulting from exposure to high alkaline and thus higher pH solutions.

Key words: Borosilicate waste glass, dissolution, alternation layer, cementitious waste forms, Ca^{2+} ions.

1.0 Introduction

Vitrification is a well-established technology for immobilizing radioactive wastes and in the US is the treatment standard for the immobilization of mixed hazardous waste particularly those resulting from defense programs. This process involves melting waste materials with glass-forming additives to incorporate contaminants within the structure of the resulting vitreous product. Borosilicate glasses are the most extensively studied and validated class of glasses used for radioactive wastes as they incorporate a wide range of contaminants and radionuclides into their amorphous structure, are less corrosive to melter components (compared to molten phosphate glasses for example), and have projected high durability in many disposal scenarios [1-2]. There are several different processes controlling the dissolution of these glasses depending on the glass composition and chemical and physical conditions near the glass surface [3]. These processes include hydrolysis of the glass network, precipitation of secondary minerals and ion-exchange (e.g., between protons/hydronium and glass alkalis ions such as Na^+ and K^+). The near field environment of the glass can dictate if these processes operate independently or intertwined with one another [3-6].

The rate of dissolution or corrosion rate can be modeled using the Transition State Theory (TST) equation [7]. The general TST rate equation used to establish chemical affinity-based kinetic rate law derives from chemical kinetics. It calculates the rate of reaction based on the slowest

elementary step in glass dissolution, which is known as the rate-limiting step [8-11]. In the case of borosilicate glasses waste forms, the corrosion behavior is primarily governed by the hydrolysis of SiO_2. In a simplified form, as silicon (Si) atom is released from the glass through hydrolysis, the concentration of Si in the near field increases. This increase in Si concentration leads to a decrease in the glass dissolution rate due to the common-ion effect. Assuming the rate-limiting reaction, the TST model can be expressed as follows [12]:

$$r_i = k_0 \ v_i \ a_{H^+}^{-\eta} exp\left(\frac{-E_a}{RT}\right)\left[1-\left(\frac{Q}{K_g}\right)^{1/\sigma}\right] \quad \text{Eq.1}$$

where r_i is the dissolution rate in g m^{-2} d^{-1} based on the element, k_0 is the intrinsic rate constant in g m^{-2} d^{-1}, v_i is the mass fraction of element i in the glass, a_{H+} is the hydrogen ion activity, E_a is the activation energy in kJ mol^{-1}, R is the gas constant as 8.314 J mol^{-1} K^{-1}, T is the temperature in K, Q is the ion activity product of the rate-limiting reaction (unitless, using Si as H_4SiO_4), K_g is the pseudo equilibrium constant for the rate controlling reaction (unitless), η is the power law coefficient, and σ is the Temkin coefficient. While this form of the TST equation is commonly represented by the behavior of Si, multiple components of the glass can influence the overall corrosion rate.

As water infiltrates a disposal facility, its chemistry changes due to interactions with various natural materials, engineered barriers, containers/canisters and the waste forms themselves. Upon contacting the glass, its chemistry is altered because dissolved species are released from the glass to the near field. As a result, the outer surface of the glass undergoes both depletion of components and bond rearrangement. As solubility limits are approached, various secondary phases may precipitate [13-14]. These processes can affect the chemical and physical properties of the altered glass surface and create a "protective" precipitates layer on a glass surface [10, 15]. Alternatively, these

phases can serve as "sinks" for dissolved species that are acting to suppress the dissolution rate, in turn lowering their concentrations and leading to an increased dissolution rate of the glass [16].

Concurrently with hydrolysis of the glass, charge balancing species in the glass network (primarily alkali species such as Na) can exchange for other protons in solution (e.g., H^+) in an ion exchange process. As the hydrolysis rate slows due to the common ion effect, the ion exchange process can be sustained leading to a continued evolution of both the near field chemistry and altered glass composition. Following the progression of the ion exchange process, an alkali-depleted zone can form a silicon-rich region, where silicon polymerization reactions can occur, forming a gel layer on the glass surface [17]. The thickness of this gel layer can vary depending on the glass composition, leaching conditions, and time [14] and can be evaluated via measurement of a cross-sectioned sample with electron microscopy or other techniques [18]. This gel layer can potentially inhibit ion exchange and shield the bulk glass from exposure to a solution, protecting it from further dissolution [19].

The chemical makeup of the infiltrating water that contributes to controlling these processes will be dictated by the source of infiltrating water, the dissolution of minerals within the near field/backfill, and the dissolution of other waste packages and/or waste forms. Cementitious materials prepared from the immobilization of liquid salt nuclear wastes are commonly referred to as "grout" [20]. Cementitious materials, both as engineering structures of a repository and as waste forms, can create an alkaline pH solution (~10-13) (called grout-contacted solution from this point on) with its dissolved constituents (e.g., portlandite, $Ca(OH)_2$, alkali content). At alkaline pH, the dissolution of SiO_2 is promoted by the attack of OH^- ions and silica monomers, $Si(OH)_4$, to form highly soluble $SiO(OH)_3^-$ and $SiO_2(OH)_2^{2-}$ ions [21]. The solubility constants of these ions are significant at pH greater than 10 with pK_1 values as -9.47 and −22.12, respectively [22]. In addition, under alkaline conditions (pH > 9), glass can have accelerated release of Al due to an OH^-

promoted dissolution mechanism and the formation of aqueous $Al(OH)_4^-$ species [23]. Consequently, an increase of pH resulting from water contacting a cementitious material can enhance the rate of glass dissolution.

A grout-contacted (GC) solution will also contain dissolved species from the hardened matrix of the cementitious materials, such as Si, Al, Ca, K. The presence of these dissolved species can alter the ion exchange processes, change precipitation or act to suppress glass dissolution. However, beyond Si, the influence of these species on glass dissolution at increased pH has been far less studied. For instance, the observed drop in the alteration rate can be attributed to the formation of silica gel that restricts water accessibility to the pristine glass surface due to a common ion effect [24-26]. Previous studies also evaluated the effect of Ca-bearing solutions on the dissolution rate and formation of alteration products at alkaline pH and 90 ^oC temperature and found a surface layer of calcium silicate hydrate (CSH) [17, 27-28]. This layer appeared to slow down the dissolution rate due to the reaction of Ca with Si in the glass hydrated surface layer. Chave et al. noted that the alteration rate was significantly reduced as calcium (Ca) concentrations increased beyond 100 mg/L [27]. Their results were consistent with measurements by [17] demonstrating that rates of glass dissolution in $Ca(OH)_2$ solution were lower compared to rates in alkaline solutions presented in literature. The formation of CSH in the presence of dissolved Ca is described as follows [29-30]:

$$2H_3SiO_4^- + Ca^{2+} \rightarrow H_6CaSi_2O_8 \qquad \text{Eq.2}$$

With the generalization of the TST model and considering the complexity of the role of near field species on glass corrosion, it becomes imperative to have real-world data on waste form dissolution in representative disposal environments.

Lysimeter tests are conducted on a larger-than-bench scale isolating soil systems which may include other materials such as waste forms and engineered barriers. These systems are then

studied under ambient environmental conditions and used to verify model predictions and compare against accelerated laboratory tests [31]. The U.S. Nuclear Regulatory Commission (NRC) has supported the operation of lysimeters for studying the degradation of radioactive waste forms. In prior work, they have noted that operating lysimeters for a minimum of 20 years will enable the prediction of waste forms stability for more than 300 years [32]. A summary of prior lysimeter tests in shallow subsurface and related to glass corrosion can be found in a recent review[31]. Currently, a field lysimeter test is underway at the Hanford site, where glass and cementitious waste forms are individually placed within disposal backfill near the planned disposal facility [33-34]. Recently the NRC commented that this current lysimeter test is "an excellent activity to provide model support for a key aspect of the performance assessment and it is strongly supported by the NRC staff"[35]. One planned configuration for this lysimeter test involves placing cementitious waste forms above glass waste forms with a backfill buffer in between. In support of this proposed arrangement and the overall understanding of the role of multiple components on glass corrosion, this study aims to investigate the impact of major elements present in a GC solution on the dissolution behavior of borosilicate glass. A combination of single pass flow-through (SPFT, ASTM C1662-18) tests and a static leach test, known as the product consistency test (PCT, ASTM C1285-21), were used to study borosilicate glass corrosion in GC solutions and solutions that varied the presence of dissolved cementitious species (Si, Ca, Al, Na, and K). Treated samples were characterized to better link the solution-based corrosion behavior and changes to the glass.

2.0 Methodology

2.1 Materials

The borosilicate waste glass used in the testing was ORLEC28, which is included in the field lysimeter test at Hanford [34, 36]. The target chemical composition of ORLEC 28 is given in Table 1.

The glass was prepared in a large, ~10 kg batch to produce waste forms for the lysimeter test. The target composition was prepared by mixing and melting known quantities of the source materials in a tilt pour furnace. The dry ingredients were mixed in a 16-quart PK Blendmaster V-blender with an intensifier for 15 minutes [37].

Table 1 Target oxide compositions and source chemicals for ORLEC28 glass waste forms.

Oxide	Source Chemical	Target, %
Al_2O_3	Al_2O_3	10.00
B_2O_3	H_3BO_3	10.00
CaO	$CaCO_3$	1.95
Cr_2O_3	Cr_2O_3	0.44
Fe_2O_3	Fe_2O_3	0.60
K_2O	K_2CO_3	3.36
MgO	MgO	1.00
Na_2O	Na_2CO_3	22.11
NiO	NiO	0.01
PbO	PbO	0.01
SO_3	Na_2SO_4	0.40
SiO_2	SiO_2	37.56
SnO_2	Na_2SnO_3	2.33
TiO_2	TiO_2	0.60
ZnO	ZnO	3.00
ZrO_2	ZrO_2	6.03
Cl	NaCl	0.20
F	NaF	0.08
MoO_3	MoO_3	0.10
P_2O_5	$NaPO_3$	0.12
Re_2O_7	$KReO_4$	0.10
Total		100.00

Glass melting was carried out using a tilt-pour induction melting furnace [UltraMELT, TLT-2P; product model: 1ACC-9000-3341-00] in conjunction with a Williamson pyrometer [model: PRO DWF-12-30] and a Watlow temperature controller. The dry ingredients were added to a 1.3 L Pt-10% Rh melting crucible at 1200 °C over a period of roughly 1.5 hours, followed by 1-hour hold time. The molten glass was poured in two segments into a pre-heated stainless steel block mold. The interior of the block mold formed a cylinder with a diameter of 3.15 inches. The cylinders were then annealed at 5 °C above the measured value of T_g (the glass transition temperature, 513 °C for ORLEC28). The glass was then cooled to 427 °C at a rate of 1.7 °C/hr,

followed by cooling to 371 °C at a rate of 3.1 °C/hr, and then to 100 °C at a rate of 10 °C/hr. Once the temperature was ≤ 100 °C, the glass cylinder was removed from the annealing oven. The cylinder was then sectioned horizontally for size reduction [34]. The bulk glass was crushed using an agate mortar and pestle and then sifted to obtain the desired size fraction 149 – 74 μm (-100 to +200 mesh). The glass powder was rinsed with deionized water (DI > 18.0 mOhm·cm) in accordance to ASTM D1193 [38] and ethanol according to the ASTM C1285-21 to remove fines [39]. The glass particles were then dried in an oven overnight at 90 °C and subsequently inspected by scanning electron microscopy (SEM) to confirm the absence of any adhered fines on the glass particles surface (Fig. S1).

2.2 Corrosion Testing

The corrosion of glass was monitored using two techniques, the SPFT [40] test and the ASTM C1285-21 for PCT [39]. The results of the SPFT test following the ASTM C1662-18 procedures, were provided in previous publications [8, 41-45]. To perform the SPFT sampling, a fraction collector, IS-95 Interval sampler with a 4-column adapter (Fischer Scientific) was used. An Isometric Peristaltic Pump (IPC Series) was employed for pumping solution into the 60 mL perfluoroalkoxy (PFA) Teflon reactors (ID: 40.8 mm, h = 63.6 mm, Savillex, Minnetonka, MN) at a controlled flow rate. The pump's peristaltic cartridges were carefully calibrated to achieve a flow rate of 28 μL/min (40 mL/day) before starting sample collection.

Three SPFT experiments were conducted under identical conditions at 25 °C, 40 °C, and 70 °C. The ratio of glass surface area to solution volume was calculated as 34.17 m^{-1}. Six blanks were collected before the addition of glass from each reactor at the same flow rate. Approximately 40-50 samples were collected from each glass reactor between 1.69 days and 6 days. Any Ca-containing

solutions were held in bag filled with N_2 to minimize the exposure to the atmosphere and precipitation of $CaCO_3$.

The PCTs were performed at 90 ^oC with solution varying the Si, Ca and/or Al concentrations. The PCTs were carried out in triplicate, and the reported results are the average values obtained from three individual reactors. In addition, as a control measure, three additional reactors were tested without glass to monitor the solutions stability at 90 ^oC. The testing reactors comprised 60 mL PFA jars with closures from Savillex, Minnetonka, MN. The experiment extended over period of 7 days at a temperature of 90±1 ^oC, maintaining a V_{soln}/m_{solids} ratio of 10:1 (equivalent to 11.0 mL solution and 1.1 g of glass), correlated to a surface area to volume (S/V) ratio of 2000 m^{-1}. After the experiment, reactors were removed from the oven, weighed, and opened for samples collection. Evaporation-induced weight changes remained less than 3% throughout the test duration. Immediately after opening the reactors, a 0.250 mL aliquot was collected from each reactor and diluted by 6.0 mL (for 3 samples) and 4.0 mL (for 2 samples) of 2 % HNO_3. Upon colling a solution to room temperature, the pH in each reactor was measured using an Orion Star A215 meter with Orion 8156BNUWP Ross Ultra electrode. Prior to pH measurements, the pH electrode was calibrated using standard pH buffers (pH 4.01, 7.00 and 10.01, Thermo Scientific). Every third reactor, aside from the glass powder, included glass coupons (approximately 1 × 1 × 5 mm^3) for cross-sectional SEM/EDS analysis (Fig. 2S). The faces of the glass coupon were polished using 180, 320, 600 and 1200 grit sandpaper and, finally, Al_2O_3 abrasive powder (with particle sizes of 1 and 0.3 μm).

2.3 Test Solution Preparation

Test solutions were a grout-contacted water (GC) and a weak buffer solution (LiOH/LiCl) adjusted to pH 12 to mimic the pH of the GC water. To ensure that the buffer solutions were chemically

similar to the GC water, their composition was adjusted based on the results of coupled plasma optical emission spectrometry (ICP-OES) analysis using a Perkin Elmer Optima 7300 DV instrument. The adjustments were made by adding specific compounds to the buffer solutions to achieve the same concentrations as those measured in the GC water (Table 2). The Ion Chromatography (IC, Dionex Integrion HPIC) analysis of the GC solution measured anion concentrations, specifically sulfate content. The GC solution was prepared by contacting deionized water (DIW, conforming to ASTM Type I[38], >18.0 MΩ·cm) with size reduced Cast Stone. Cast Stone is a cementitious waste form made with 47 wt. % ground granulated blast furnace slag, 45 wt. % class F fly ash and 8 wt. % ordinary Portland cement mixed, in this case, with simulated Hanford low-activity waste (LAW). The fabrication of Cast Stone is covered elsewhere [46]. The cured Cast Stone was crushed to < 2 mm and contacting 25.0 g of powdered grout with 1.0 L of DIW for 7 days on a mechanical shaker at 70 rpm, after which the solution was filtered via 0.45 μm vacuum filter to remove the solids. The filtrate characterized by a pH 12.40 ± 0.08 was used as a GC solution; its measured chemical composition analyzed via ICP-OES is given in Table 2. Ca^{2+} ions were found to be the major ionic species in the GC solution.

X-ray diffraction (XRD) was used to characterize the grout powder before and after it was in contact with water (Fig. S10). Table S2 summarizes crystalline phase compositions of each powder obtained by fitting XRD patterns (i.e., amorphous phases are not included). The major phases in the original grout consisted of calcite, gypsum, quartz and ettringite. Upon contact with water to produce the leachate, the ettringite phase disappeared, and a substantial percentage of vaterite was formed. Vaterite, a metastable form of calcium carbonate, has higher solubility in water compared to either calcite or aragonite. However, vaterite is unstable and slowly reverts to one of these phases with time. The dissolution of ettringite and calcium carbonate polymorphs could potentially

increase sulfate (SO_4^{2-}) and Ca concentrations in a GC solution. This can influence the glass dissolution behavior by creating a CSH surface layer and calcium -bearing precipitates on the surface of the glass particles.

Table 2 Chemical composition of a GC solution via ICP-OES and IC analysis. Note: Average values were calculated based on measurements of four samples.

Analyte	mg/L
Si	6.35
Na	28.73
K	28.54
Ca	132.33
Fe	1.34
Al	6.75
SO_4	31.50
Cl	1.08

SPFT tests were performed using a baseline control reactor with a pH 12-adjusted buffer solution (LiOH/LiCl), as well as with the GC solution or the pH 12 buffer chemically adjusted with either Na_2SiO_3 (5 mg/L of Si) or $CaCl_2$ (130 mg/L Ca) (Table 3). These concentrations were chosen to be equivalent to the concentrations found in the GC solution.

PCTs were performed using the following solutions: (i) a pH 12-adjusted buffer as a control, (ii) the GC solution, and (iii) five leachate solutions prepared in pH 12 buffer with a composition outlined in Table 3. All solutions were buffered by LiOH/LiCl to pH 12.

Table 3. Leachate solutions prepared for SPFT and PCT experiments.

	Description	Acronym	Concentration, mg/L
		SPFT Tests	
1	pH 12-adjusted buffer solution		LiOH/LiCl, reactor R1
2	Grout-contacted solution	GC	Duplicate reactors, R2, R3
3	pH 12 buffer adjusted with Na_2SiO_3	BA12-Si	5 mg/L of Si, duplicate reactors R2, R3

4	pH 12 buffer adjusted with $CaCl_2$	BA12-Ca	130 mg/L Ca, duplicate reactors R2, R3
		PCT Tests	
1	Na_2SiO_3	SiO_3^{2-}	5 mg/L Si
2	$CaCl_2{\cdot}2H_2O$	Ca	130 mg/L Ca^{2+}
3	$CaCl_2{\cdot}2H_2O + Na_2SiO_3$	Ca+ SiO_3^{2-}	130 mg/L Ca^{2+} + 5 mg/L Si
4	$Al^{3+} + Na_2SiO_3$	Al+ SiO_3^{2-}	7 mg/L Al^{3+} + 5 mg/L Si
5	$Ca^{2+} + Al(NO_3)_3{\cdot}9H_2O + Na_2SiO_3$	Ca+Al+SiO_3^{2-}	130 mg/L Ca+ 7 mg/L Al^{3+}+ 5 mg/L Si
6	GC solution	GC	Data in Table 2

A pH 12 buffer solution was prepared by dissolving LiCl and LiOH (purchased from Fischer Scientific) in DIW. Sodium metasilicate nonahydrate ($Na_2SiO_3{\cdot}9H_2O$, 44-47.5% total solids, Fischer Scientific), calcium chloride dihydrate ($CaCl_2{\cdot}2H_2O$, certified ACS from Fisher Chemicals), and aluminum nitrate nonahydrate ($Al(NO_3)_3{\cdot}9H_2O$, certified ACS from Fisher Chemicals) were used to prepare silicon-, calcium- and aluminum-amended solutions with concentrations of 5 mg/L Si, ~130 mg/L Ca, and 7 mg/L Al), respectively. Analytical measurements were conducted using 1%-2% diluted nitric acid (Trace Metal grade, 67-70 wt. %)

2.4 Solutions Analysis and Calculations

The concentrations of boron (B) and rhenium (Re), used as indicator for glass dissolution monitoring, were determined with inductively coupled plasma mass spectroscopy (ICP-MS, Thermo Fisher Scientific, iCAP RQ). The calibration of ICP-MS was performed with 3 replicates, a dwell time of 0.1 s, a wash time of 30 s, and a delay time of 30 s. Boron was selected as the glass dissolution tracer due to its presence as a glass forming element that is not retained in the alteration products [47-49]. Re was used as a substitute for Tc, which is present in actual LAW glass forms. Measurements of Si, Al, and Ca were performed using ICP-OES. The estimated limits of quantification (LOQ) for B and Re by ICP-MS were 0.212 μg/L and 0. 003 μg/L, respectively. The LOQ for Si determined by the ICP-OES was 50 μg/L.

Concentrations used to calculate the dissolution rates of elements were obtained when the system reached equilibrium, where the concentrations of elements released from the glass had not changed with respect to time. The mean deviation between values in a plateau region was less than 10%, which is within the experimental error calculations. The normalized mass loss, NL*(i)*, g m^{-2} for each element, *i*, was calculated as follows:

$$NL(i) = (Ci - Cib)/[fi(SA/V)] \quad \text{Eq. 3}$$

where C*i* is the average concentration of *i* element in solution in the duplicate experiments and *Cib* is the average concentration of *i* in the blank tests (both in g m^{-3}); f*i* is the mass fraction of *i* in the glass monolith (unitless); SA is the surface area of the glass powder (in m^2); and V is the volume of solution (in m^3) [50].

2.5 Characterization

Micrographs and elemental analysis of used glass coupons from each experiment were captured using a JEOL JSM-5900LV scanning electron microscope equipped with energy-dispersive X-ray spectroscopy (SEM/EDS) at 25.0 kV and a takeoff angle of 35.0°. For the SEM/EDS investigation, the glass coupon samples were embedded in epoxy resin and polished using Al_2O_3 abrasive powder (Fig. 2S). To prevent surface charging under the electron beam, the specimens were coated with a layer of gold using a cold sputter coater. The collected data were quantified via the Bruker Esprit software. Elemental mapping was conducted at a distance of 10 nm with a measurement time of 600 second.

X-ray diffraction measurements of glass and grout powders were conducted using a Bruker D2 PHASER X-ray diffractometer equipped with LYNXEYEXET (1D mode, opening 5° 2θ) detector and a rotating collimator source. The diffractometer was operated at 30 keV and 10 mA, with a temperature of 297 K. The samples were loaded onto zero diffraction plates (Ø 24.6 mm × 1.0 mm

thickness with cavity Ø 10 mm × 0.2 mm depth, MTI Corporation) and scanned from 5° to 90° with a step size of 0.02°and a duration of 1s per step. The solid phase identification was conducted using the *Match!* XRD pattern processing software.

The Brunauer-Emmett-Teller (BET) surface area and pore distribution measurements of treated glass samples were conducted in triplicates. Nitrogen adsorption-desorption isotherms were acquired at 77 K using a gas adsorption analyzer (Micromeritics TriStar II 3020 V1.03). Approximately 1 g of glass particles were degassed with nitrogen gas at 353 K for 24 h. The specific surface area was determined using the Brunauer–Emmet–Teller (BET) equation (Brunauer et al., 1938) considering the cross-sectional area of monolayer adsorbed nitrogen (0.16 nm^2). The Barrett, Joyner, and Halenda (BJH) procedure, based on the Kelvin model of pore filling, was used to calculate the pore size distribution from experimental isotherms.

The BET specific surface area according to [33] for the prepared glass powder with the average particle size of 5.63×10^{-5} m (-100 to +200 mesh or 74–149 μm) was calculated as $2.04 \times 10^{-2} \pm 0.005$ m^2/g, which is in a good agreement with values calculated from geometrical size. Glass bulk density was 2.74 g/cm^3 [33].

2.6 Speciation modeling

Geochemical modeling was used to predict the formation of saturated mineral phases and aqueous species, including borate species, in the experimental solutions. The speciation diagrams predicting the formation of aqueous species and saturated indices of possible precipitates were calculated via Geochemist's Workbench modeling software (GWB, version 12.0). The concentrations of ions measured in the leachates (Table S1) were used for series modeling variations with initial concentrations outlined in Table 3: Si- 0.18 mM (5 mg/L), Al-0.26 mM (7 mg/L), Ca^{2+}-3.24 mM (130 mg/L, balance on Ca^{++}), and sliding pH in the range of 11.5 – 12.0.

The composition of the GC solution in the GWB React mode was adjusted with 31.5 mg/L of sulfate (SO_4^{2-}), as measured in liquid analysis by the IC instrument (Table 2).

PCT's were conducted at 90 °C but speciation modeling for comparison between solution compositions was conducted at a constant temperature of 25 °C due to the system oversaturation and unavailability of some stability constants for the formation of metal complexes at 90 °C. These simulations used a thermo.com.V8.R6+ database included in GWB.

3.0 Results

3.1 Corrosion Testing

3.1.1 Single-Pass Flow-Through (SPFT) Experiments

The SPFT experiments utilized one of the leachate solutions whose composition is outlined in Table 3. The normalized dissolution rates (NDR) of Re (NDR_{Re}) and B (NDR_B) for different leachates measured at the three studied temperatures, 25 °C, 40 °C, and 70 °C increased with rising temperature (Fig. 1). For instance, the NDR_{Re} and NDR_B in the buffer control in Reactor 1 (R1) were calculated as 0.01 g $m^{-2}d^{-1}$ at 25 °C, 0.02 g $m^{-2}d^{-1}$ at 40 °C and 0.20 g $m^{-2}d^{-1}$ at 70 °C for Re and 0.01 g $m^{-2}d^{-1}$ at 25 °C, 0.03 g $m^{-2}d^{-1}$ at 40 °C and 0.18 g $m^{-2}d^{-1}$ at 70 °C for B. The NDR_B and NDR_{Re} in the pH 12 buffer were significantly higher than those in the GC solution, with calculated values of 0.001 g $m^{-2}d^{-1}$ at 25 °C, 0.02 g $m^{-2}d^{-1}$ at 40 °C and 0.03 g $m^{-2}d^{-1}$ at 70 °C for Re and 0.001 g $m^{-2}d^{-1}$ at 25 °C, 0.0053 g $m^{-2}d^{-1}$ at 40 °C and 0.008 g $m^{-2}d^{-1}$ at 70 °C for B. When attempting to isolate the species in the GC solution responsible for the suppressed rates, the NDR_B and NDR_{Re} in BA12-Si solutions were similar to the rates measured in the pH 12 buffer. This observation shows the assumed common ion effect accounted for in the TST model based on only Si may not be representative at high pH due to speciation changes of Si where orthosilicic acid is no longer the dominant species. Ca is a significant component of the grout contacted solution. The addition

of Ca to the pH 12 buffer at the same concentration as the GC solution lowered the NDR for both Re and B below the GC solution NDR values at room temperature. At the two higher temperatures, the NDR values were slightly greater for the Ca-amended solution than the GC (Fig. 1).

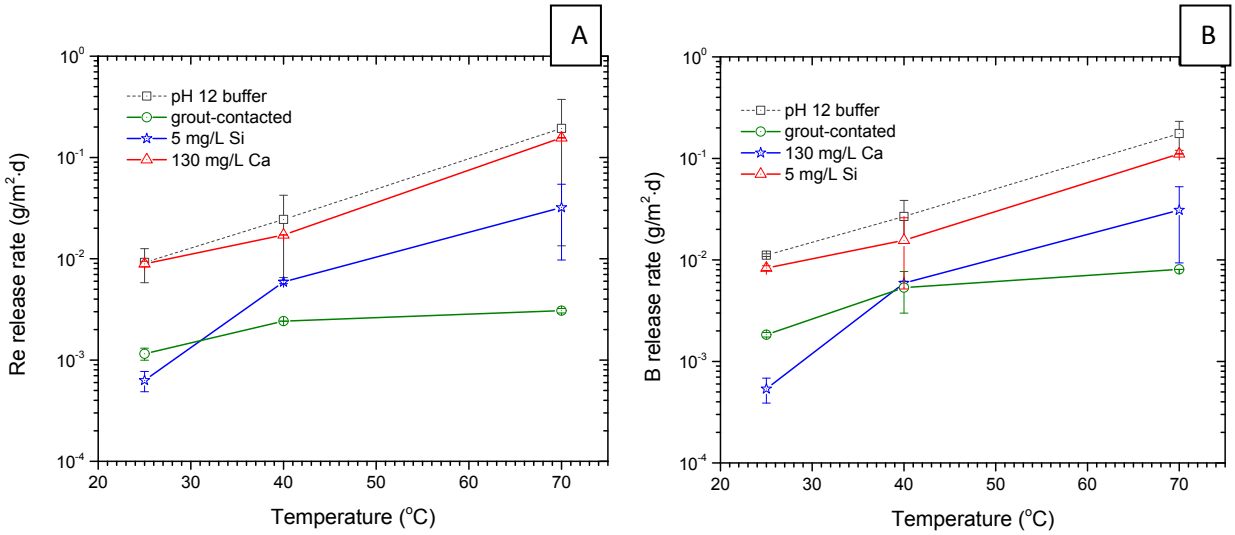

Fig. 1. Normalized dissolution rates with respect to Re and B as a function of temperature in SPFT experiments performed in different leaching solutions: (grey squares) pH 12 buffer; (green circles) grout-contacted, (blue stars) pH 12 buffer amended with 5 mg/L Si (0.18 Mm), and (triangles square) pH 12 buffer amended with 130 mg/L of Ca (3.24 Mm). Note: Reactor 1 is a pH 12 buffered solution; reactors R2 and R3 are identical duplicate reactors with GC or pH 12 buffer leaching solutions amended with Si or Ca^{2+}. The presented release rate values are averages between duplicate reactors R2 and R3.

3.1.2 PCT

PCT's at 90 °C were performed to refine the understanding of the reduced NDR observed in GC solution by SPFT, compare the effect of various elements within the GC solution and obtain samples for the analysis of the glass surface after corrosion. The results indicated that the normalized loss (NL) rates were significantly reduced compared to the pH 12 buffer for both NL_B (one order of magnitude) and NL_{Re} (two orders of magnitude) in both the GC solution, BA12-Si, and BA12-Ca. For instance, in Ca^{2+}-bearing leachates or Ca+Si leachate solutions, the NL for all species was equal to or lower than the NL in the GC solution (Fig. 2, a-f). Speciation modeling supported the presence of dissolved Ca^{2+} in high pH leachate solutions, which promotes the

formation of strongly bonded calcium-silicate hydrate (CSH) layers on the glass surface according to Eq.2 (Maraghechi et al., 2016) (Fig. S3). However, the presence of Al^{3+} slightly increased the NL above that of the Ca-amended or Ca-Si-amended solutions.

Amending the pH 12 buffer with Si alone or in combination with Al^{3+} in the leachate solutions does not significantly affect the NL (Fig. 2a, b). The small reduction of NL in the Al^{3+} + SiO_3^{2-} solution compared to the baseline pH 12 control can be explained by the difference in the solid phases formed under experimental conditions in the presence of Al/Si and saturation indices predicted under equilibrium conditions in GWB simulations (Fig. 2a, b; Fig. S3). In the Ca+Al+SiO_3 amended solution, the NL(Re) is notably higher than NL(B). Both Re and K exhibit similar trends across the different solutions (Fig. 2b, f). Speciation modeling conducted at 25 °C did not predict any saturated phases with B, and modeling at 90°C was not feasible due to the system oversaturation. It is plausible that B is being retained or precipitated in the alteration layer or corrosion product within the Ca+Al+SiO_3 solution test resulting in a lower aqueous concentration of B.

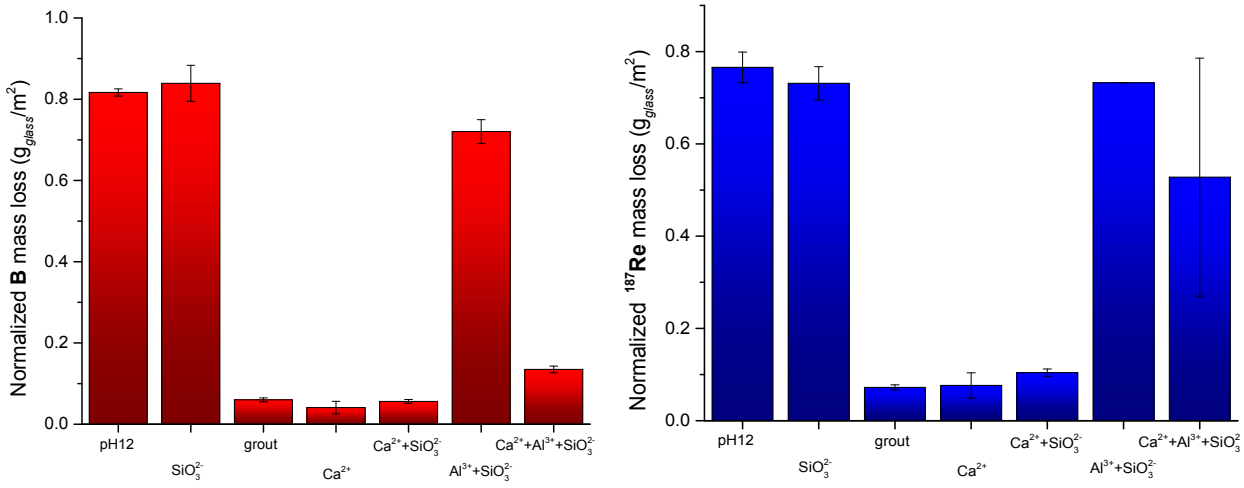

a) b)

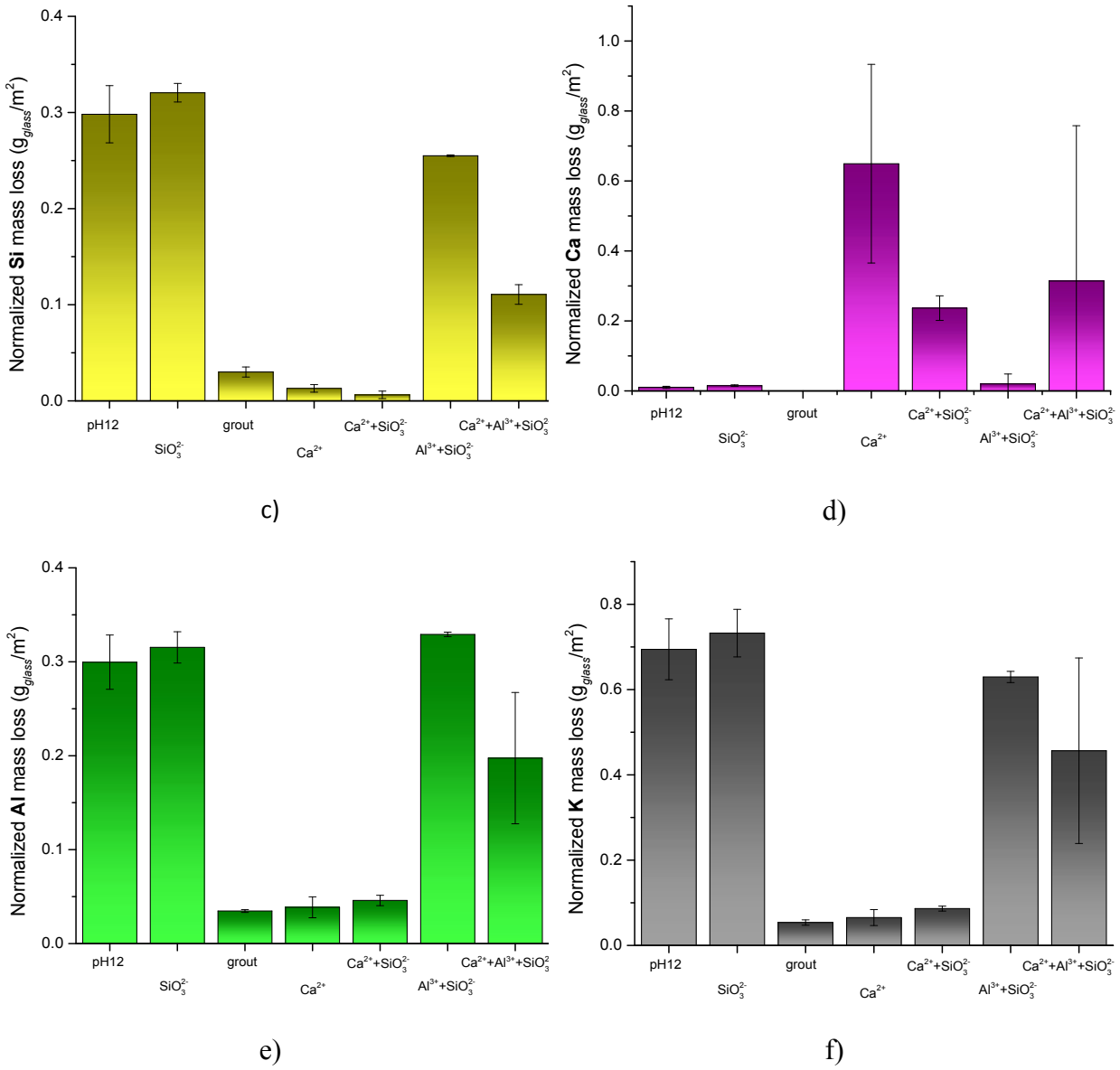

Fig. 2 Normalized elemental losses of B, Re, Si, Ca, Al, and K calculated after analysis of the leachates collected after 7 days PCT static test at 90 °C in different solutions.

3.1.3 Speciation modeling of experimental solutions.

A Geochemist Workbench (GWB) equilibrium speciation model was utilized to predict the formation of major aqueous and saturated solid species in the PCT reactors and to trace changes in concentration of borate species (Fig. S3-Fig. S9). The formation of precipitates has the potential to inhibit the extent of dissolution due to their stabilizing effect on the altered glass surface. The

geochemical modeling results indicated the speciation of both borate anion and Ca-borate cation when an abundant amount of Ca is present, which correlates well with the observations in the SPFT and PCT experiments (Fig. S3-S9).

In the Ca-free leachate solutions at pH 12 and containing SiO_3^{2-}, the predicted borate aqueous species were tetrahydroxyborate $B(OH)_4^-$, $CaB(OH)_4^+$, $NaB(OH)_4$, and $B(OH)_3(aq)$ (Fig. S3, S4). The formation of $CaB(OH)_4^+$ species was three times less compared to $B(OH)_4^-(aq)$, likely due to the low concentration of Ca less than 0.5 mg/L in the aqueous phase (Table S1). The model predicted saturation with respect to grossular and wollastonite. The aqueous Si concentrations in the SiO_3^{2-} and Al^{3+} + SiO_3^{2-} solutions were measured as 0.39 mM compared to the initial 3.65 mM amended leachate solution, suggesting a saturation of aluminosilicate phases with respect to potassium feldspar (K-spar) $KAlSi_3O_8$, microcline $KAlSi_3O_8$, kalsilite ($KAlSiO_4$), prehnite $Ca_2Al_2Si_3O_{12}(OH)$, and close to saturation grossular (Fig. S4, S5). The GWB thermodynamic modeling indicates that at pH 12, which is initial pH of tested Al^{3+} + SiO_3^{2-} solutions prepared for the PCT experiments, aqueous Al^{3+} remained as AlO_2^- (Fig. S5). A minimal change in pH was observed in PCT testing (Table S3).

The presence of Ca in a GC solution and pH 12 buffer solutions, amended by Ca^{2+} or Ca^{2+} blended with SiO_3^{2-}, predicted the predominant boron species in the aqueous phase. The distribution included $B(OH)_4^-$ at concentrations ranging from 0.19 mM to 0.27 mM, $CaB(OH)_4^+$ at concentrations from 5.15e-02 mM to 6.91e-02 mM, and the formation of $B(OH)_3(aq)$ species at concentrations from 2.75e-04 mM to 3.94e-04 mM (Fig. S6-S7). In the Ca+Si+Al- amended leaching solution, modeling predicted the formation of aqueous borate BO_2^- at 0.54 mM and low concentrations of $B(OH)_3(aq)$ at 8.350e-04 mM and $CaB(OH)_4^+$ at 2.53e-04 mM. The saturated species were prehnite, kalsilite, and close to saturation grossular (Fig. S8). The modeling of the

GC solution predicted the saturation of grossular, phyllosilicate antigorite, and calcite but undersaturation of the gypsum solid phase (Fig. S9). The B speciation results, showing the presence of borate and Ca-borate at alkaline pH, are in agreement with previous literature on B speciation in basic conditions [51-52].

3.2 Post-corrosion glass characterization

3.2.1 SEM/EDS analyses

The post-experiment PCT glasses (pH12, Ca-amended and GC solutions) were examined using SEM/EDS. Glass exposed to the pH 12 buffer solution exhibited corrosion pockets in the form of deep holes with a diameter of 200-300 μm, covering the glass particles surface (Fig. 3A). In contrast, glass particles treated in the Ca-amended solution showed no sign of surface corrosion compared to the untreated glass sample (Fig. 3B). Lastly, glass particles treated in the GC solution featured minor corrosion defects appearing in the form of shallow pits of irregular shape with a diameter of about 500 μm (Fig. 3D). These minor corrosion pits were observed on only a limited number of glass particles (Fig.3D).

Fig. 4shows SEM images of glass particles at high magnification. Surface of the glass particles treated in treated in grout-contacted and Ca-amended solutions is clean from any precipitated phases. Contrary, the surface of glass particles treated in pH 12 buffer solution is covered with worm-like precipitates of ca. 200 microns length.

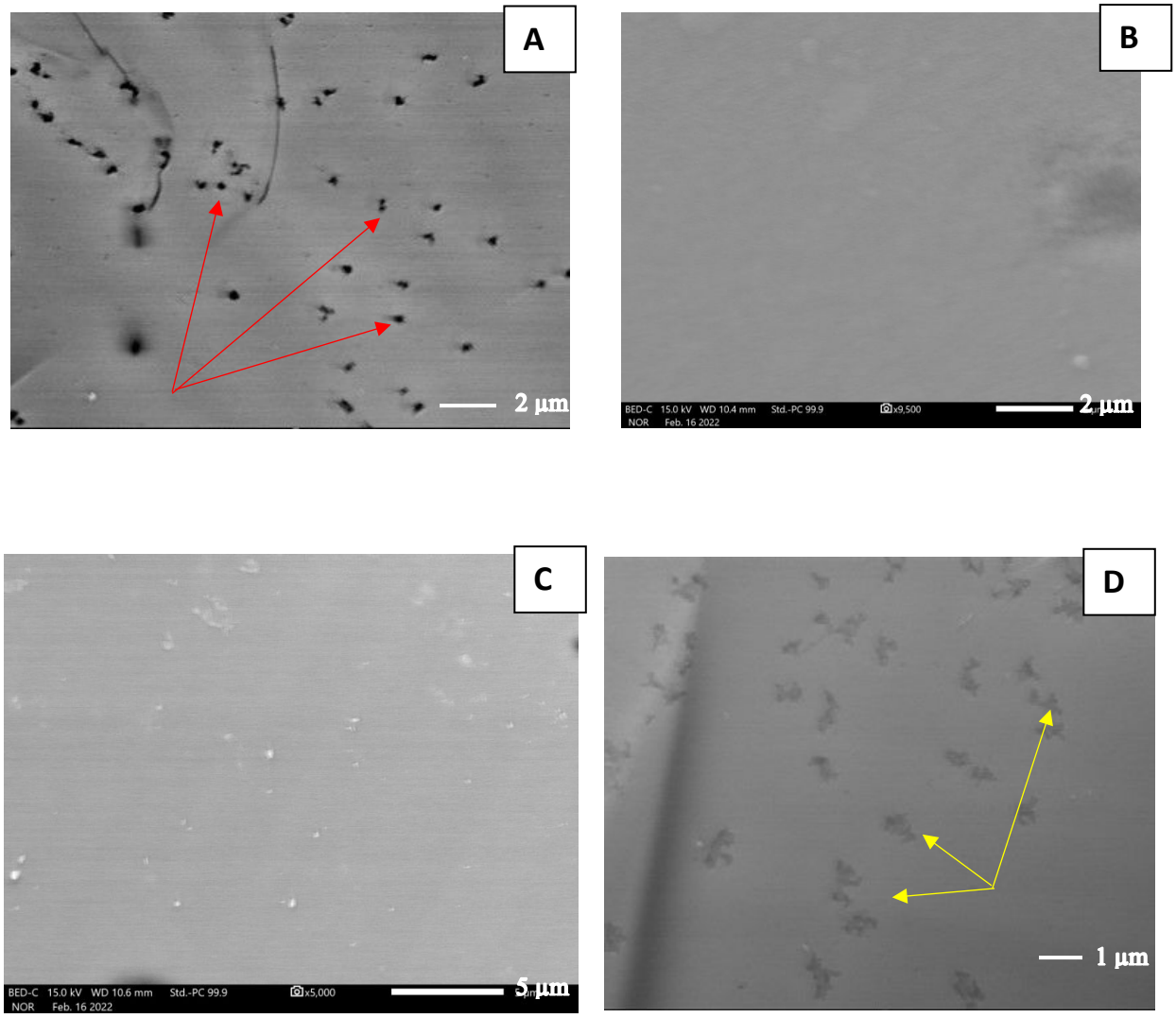

Fig. 3 SEM images of the glass particles used in the static PCT test. A) deep corrosion pockets on the surface of glass treated with pH 12 buffer solution (indicted by red arrows); B) glass treated with Ca^{2+} solution buffer solution; C) glass in contact with a GC solution; D) minor corrosion pits observed on the glass surface when exposed to a GC solution (indicated by yellow arrows).

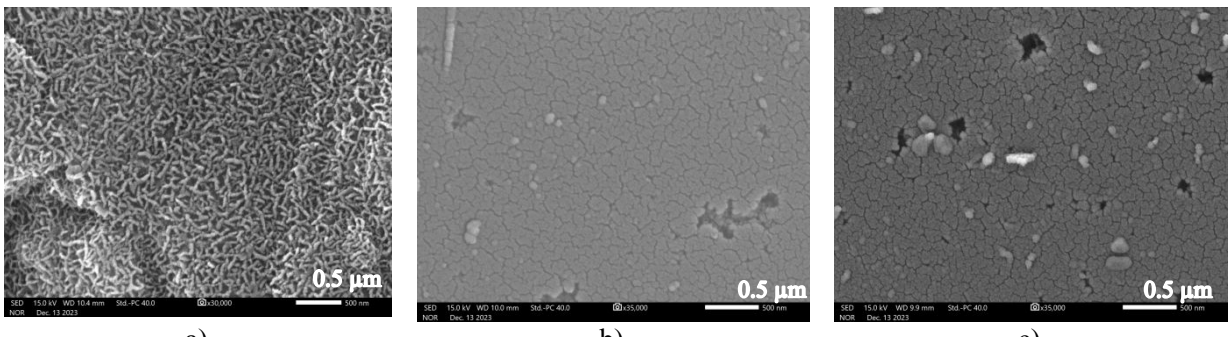

a) b) c)

Fig. 4SEM images at 10,000-15,000 magnifications of glass powders treated in PCT: (a) pH 12 buffer, (b) GC,and (c) Ca-amended solutions.

The results from the SEM testing revealed a significant decline in glass corrosion defects after treatment in grout or Ca-amended leaching solutions. This reduction positively correlated with a significant decrease in the cumulative volume of glass pores, as determined by the BJH adsorption procedures (Table 4). Additionally, the SEM analysis identified precipitates with crystal rhombohedral morphology on the surface of glass particles treated in a GC solution (Fig. 5). Based on the EDS analysis, the identified precipitates are calcium carbonate polymorphs, specifically calcite and aragonite. The detection of calcite by SEM/EDS after PCT of glass treated in a GC solution correlates with the results of speciation modeling (Fig. 5).

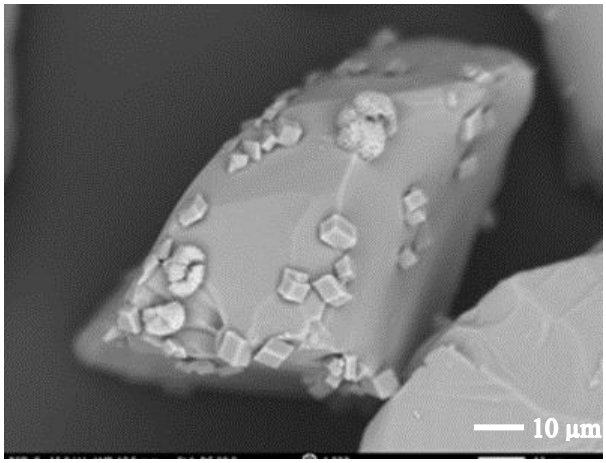

Fig. 5 Crystalline deposits observed on the surface of glass particles subjected to the static PCT test using GC solution.

3.2.2 BET surface area and porosity measurements.

BET surface area and pore size measurements were conducted for both pristine and corroded glasses (pH 12 buffer, grout-contacted, Si-, or Ca-amended solutions) (Table 4). The results showed that the specific surface area increased after the PCT. The pH 12 buffer produced the highest surface area (an increase of 197 times compared to the pristine glass), followed by the Si-amended solution (89 times higher than pristine), the Ca-amended solution (30 times higher

than pristine), and the GC solution glass showed the lowest increase in surface area (18 times higher than pristine). An increase in the BET surface area after the static experiment may be attributed to the etching of the glass surface during the test or the precipitation of secondary phase fines on the surface of glass particles. Furthermore, there was a substantial decrease, about 2,000 to 3,000 times lower, in the volume of the pore size between 17 Å and 3000 Å in BJH measurements for the glass powders treated in GC and Ca-amended solutions compared to BET parameters of glass treated in pH 12 buffer solution (Table 4). The latter observation suggests the potential closure of smaller pore voids in the presence of Ca^{2+} ions, possibly attributed to the precipitation of CSH or other corrosion products like calcium carbonate derived from the saturated grout solution. CSH corrosion products may have formed a surface layer with lower porosity and smaller pore size that can contribute to the slower kinetics of glass dissolution observed in SPFT and static PCT tests [29, 53]. With respect to BET surface area and pore volume measurements via nitrogen adsorption, it is important to note that some measured values are at the detection limit of the instrument (Table 4). These nitrogen-BET surface area values are lower compared to those measured by BET krypton adsorption[13]. Glass particles from PCT, characterized by XRD, do not exhibit any mineralogical changes compared to the pristine glass (Fig. S11). This could be attributed to the low content of alteration products formed on the glass surface or the newly formed phases may be amorphous, making them challenging to detect using the XRD method employed in this study.

Table 4 BET surface area and cumulative pore volume of glass powders used in the duplicate static test at 90 °C. Note: results are average values of two measurements for each sample.

Sample ID	BET surface area, m^2/g	BJH adsorption cumulative pore volume between 17.000 Å and 3000.000 Å width, cm^3/g
Pristine glass	<0.01	0.0090 ± 0.0009
pH12	0.79 ± 0.01	0.8912 ± 0.008

Grout-contacted solution	0.08 ± 0.01	0.0003 ± 0.0004
Si-amended solution	0.35 ± 0.01	0.4173 ± 0.008
Ca^{2+}-amended solution	0.12 ± 0.01	0.0004 ± 0.00006

3.2.3 The alteration layers' composition on the treated glass

Both the measurement of the thickness layer and the porosity of treated glass coupons are important features in glass corrosion studies [18]. 1-D concentration profiles of major elements as a function of a distance from the edge of a glass coupon were obtained by EDS cross sections after PCT testing in variable alkaline aqueous solutions. An alternation layer of approximately 4 μm thickness was measured in a coupon from the pH 12 buffer, as evidenced by the depleted amount of Na, K, and Si (Fig. 6A and Fig. 6D). Notably, that K concentrations in the glass recover within about 2.9 μm distance from the edge of the glass coupon, while the depletion depth of Na extends to about 4 μm based on 3-4 measurements of 2 samples. This observation can be attributed to the difference in diffusion coefficients for Na and K within the glass [54]. In the pH 12 buffer amended with Si, an alternation layer about 3 μm thickness was observed, with the once again noted difference in Na and K depth (Fig. 6B). Analysis of the coupon from the GC solution revealed: (1) a much thinner alternation layer (thickness ~1 μm - 3 μm) compared to the other two glass coupons treated in pH 12 buffer and Si-amended pH 12 buffer, suggesting that the depth of corrosion compared to the original surface is much lower in the GC (Fig. 6C); (2) unlike the previous samples, Na and K become enriched at the outermost surface in the alternation layer compared to the rest of the altered region. This Na/K enrichment corresponded to a depletion of Si in the same region (Fig. 6C, 6F); (3) the outermost portion of the alternation layer was enriched with Al (Fig. 6F). These results confirm that the surface behavior in a GC solution significantly differed from

the other two solutions at the same pH and that other elements in addition to silicon in the solution can affect glass dissolution.

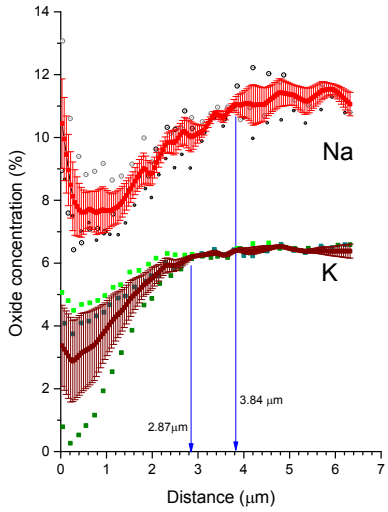

a) pH 12

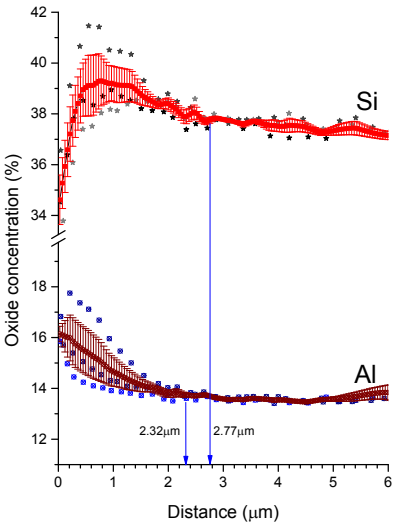

d) pH 12

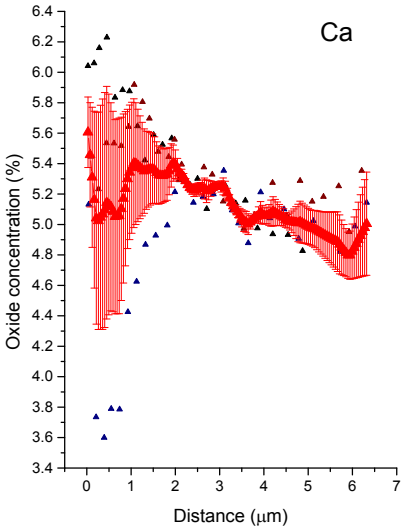

g) pH 12

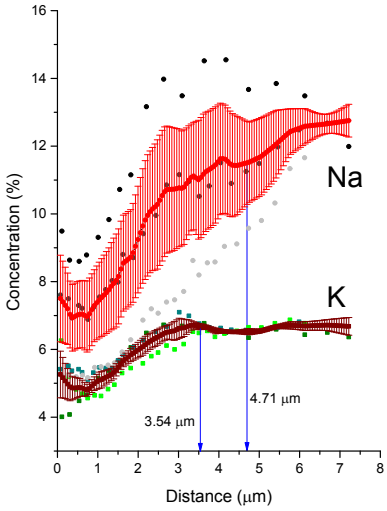

b) Si-amended

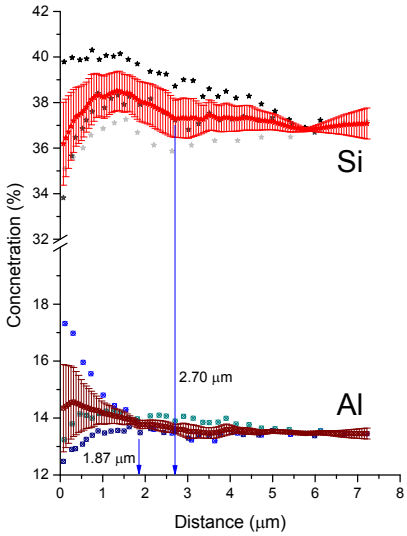

e) Si-amended

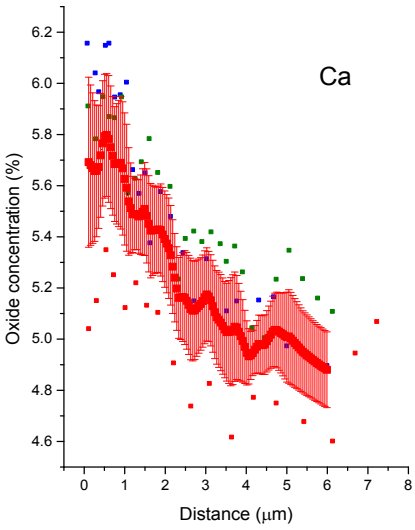

h) Si-amended

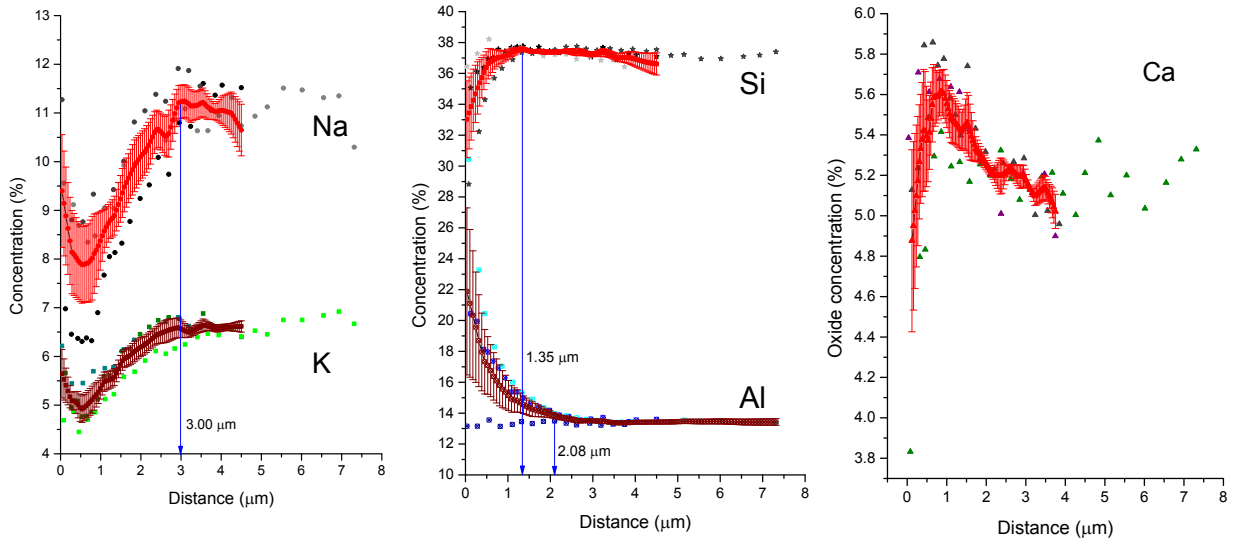

c) GC f) GC i) GC

Fig. 6 The distribution of major elements as a function of distance from the coupon's edge obtained by EDS cross sections after PCT testing. A glass coupon was collected after PCT experiment conducted at 90 °C:(a)-(c) Na and K concentration profiles in glass coupons treated in pH 12 (a), (b) Si-amended solution and (c) GC solution; (d)-(e) Si and Al concentration profiles in glass coupons treated in pH 12 (d), (e) Si-amended solution and (f) GC solution; (g-i) Ca concentration profiles in glass coupons treated in pH 12 (g), (h) Si-amended solution and (i) GC solution.

Table 5 lists alternation layer thickness for Na, K, Si, Al, and Ca measured by EDS on glass coupons treated in all solutions studied in this work. An alternation layer is clearly observed by depleted Na and K concentrations of the glass specimens treated in pH 12 and Si-amended solutions, with an estimated thickness of the alternation layer up to ~5 μm. In contrast, the treatment of glass in GC and Ca^{2+}-amended solutions has a much weaker effect on the thickness of the glass surface alteration inducing an enrichment with Ca to an average depth of about 2.5 microns. Furthermore, in the Ca-amended solution, the Ca concentration was higher at the edge of the glass specimens but then reduced with distance.

Table 5 Alternation layer thickness, μm, for different elements in the static PCT test at 90 °C.

Solution	**Na**	**K**	**Si**	**Al**	**Ca**
pH 12	-3.84	-2.87	-2.77	+2.32	-1.00

Grout-contacted	-3.00	-3.00	-1.35	+2.08	+2.5
SiO_3^{2-}	-4.71	-3.54	-2.70	+1.87	-0.9; +1.6
Ca^{2+}	-4.05	-3.31	-1.84	-1.6	+3.3
Ca^{2+} + SiO_3^{2-}	+0.85; -3.5	+0.72; -3.5	-0.91	-0.84	+2.05
Al^{3+} + SiO_3^{2-}	-4.4	-3.8	-1.2	-0.71	0.0
Ca^{2+} + Al^{3+} + SiO_3^{2-}	-4.15	-3.36	0.0	0.0	+2.2

Note: Negative sign corresponds to decreased concentration of the element compared with its concentration in the bulk glass and positive sign corresponds to the increased amount of the element compared with the concentration in the bulk glass.

4.0 Discussion

This study expanded the knowledge of the role other elements, beyond Si, play in the corrosion behavior of nuclear waste glasses. The results from the SPFT experiments suggest that Ca plays a role in the suppression of glass corrosion, in a multi-component common-ion effect with other minor dissolved components at high pH. This finding aligns with data reported by Mercado-Depierre et al. (2013), which also showed that Ca-enriched solutions have a retarding effect on glass dissolution mechanisms [55]. The influence of Ca was also observed in kinetic measurements of soda-lime glass dissolution in highly alkaline NaOH solutions by [29]. Their results indicated a decrease in the dissolution rate attributed to the formation of a dense, low porosity, and strongly bonded CSH layer on the glass surface. Previous research has suggested that if the pore water composition in contact with glass is dominated by cement species, the formation of calcium-silicate-hydrates may occur due to a strong affinity between Ca and Si gels in alkaline environments [53, 56]. In addition, Backhouse et al, 2019[50] investigated the impact of aluminoborosilicate glass compositions, particularly the Mg or Ca content, on glass structure and dissolution behavior in high pH conditions. They found similar corrosion rates for both Ca- and Mg-containing glasses. In the presence of Ca, both Fe and Mg can be incorporated into the gel layer; however, the relative proportion of Ca in the gel is higher than that of Fe and Mg [49].

The results from the PCT measurements validate the findings from the SPFT experiments. Specifically, the PCT measurements revealed a reduction in the NL rates in GC solution when compared to the pH 12 buffer. This reduction is consistent across various factors including NL_B and NL_{Re} in both the GC solution, BA12-Si, and BA12-Ca. The speciation modeling demonstrated a strong correlation with the observations made in the SPFT and PCT experiments. In alkaline pH conditions, the glass surface carries a negative charge. This electrostatic property plays an important role in the preferential adsorption of divalent Ca cations onto Si-rich surface sites [23]. The interaction between dissolved Ca^{2+} and Si-rich amorphous glass within the hydrated surface layer results in significant alterations occurring on the surface of silicate glasses and the formation of a CSH passivation layer [17]. The formation of this CSH layer in alkaline pH conditions is an important factor affecting glass corrosion. This alteration layer, enriched with Ca^{2+}, may serve as a protective barrier that can impede further corrosion of the glass substrate. Further analysis of the distribution of major elements in samples treated in the solutions containing Ca showed enrichment of Ca on the surface, while Si and Al were depleted in the same regions compared to the bulk glass. Although other observations [57] have demonstrated that solutions enriched with calcium influence glass alternation by precipitation of either calcium borate or calcium silicate hydrates, our results suggest the immediate surface is dominated by Ca. All Ca-bearing solutions predicted the formation of $CaCO_3$(aq), and the GC solution aqueous species also included $CaSO_4$(aq) with gypsum being undersaturated. The most prevalent saturated mineral phases in the GC and pH 12 solution amended with Ca^{2+}, Al^{3+}, and SiO_3^{2-} were grossular ($Ca_3Al_2(SiO_4)_3$, calcium carbonate polymorphs ($CaCO_3$) such as calcite, kalsilite, and prehnite, respectively (Fig. S8, S9). The speciation modeling did not predict the formation of borosilicate, possibly due to insufficient thermodynamic data available for boron-bearing minerals in the literature. However, the formation

of boron-bearing minerals is feasible, as boron has been known to create many independent minerals, with BO_4 groups frequently linking to SiO_4 groups, forming chains, sheets, and frameworks [58]. There also are indications in the literature that boron can be incorporated into silicate-hydrate phases [59-60]. It is also known that boron can be integrated into crystalline CSH phases in significant amounts, facilitated by the presence of Ca, as seen in the mineral oyelite, a hydrous calcium borosilicate $Ca_5BSi_4O_{13}(OH)_3 \cdot 4H_2O$, which belongs to the tobermorite group [61-62]. Additionally, B retention in the gel was found to be highly favored in basic pH, and the co-presence of Ca and B in the solution provided protection for the glass surface by significantly reducing the alteration rate of glass. This result was obtained by conducting adsorption experiments using silica and an aqueous solution of $B(OH)_3$ at 7,000 mg/L for B, and $CaCl_2$ at 7000 mg/L for Ca [63]. These concentrations are almost two orders of magnitude larger than the concentrations used in this study; therefore, the results might not be as pronounced.

The efficient adsorption of borate onto clay minerals at elevated pH in a Ca-rich environment or when pH is adjusted by Ca solutions has been well documented [64-65]. This effectiveness is attributed to the formation and subsequent adsorption of $CaB(OH)_4^+$ ions [64]. The negatively charged interlayer sites between sheets of clay minerals favor the attraction of the positively charged Ca-borate cation, which depends on pH and concentration of B [51]. However, it is important to note that previous experiments examining borate adsorption on clay were carried out at considerably higher concentrations of Ca and B compared to the concentrations used in the present study (Table 2, Table S1). This difference in concentration levels may impact the observed adsorption effects of boron [66]. This is important in the context of co-precipitation of boron-bearing minerals, which were not observed by the solids characterization methods used in this study.

The results indicate that Ca plays a prominent role in the enrichment of the CSH layer or precipitate as Ca secondary phases on the surface. These results suggest that Ca diffusion from the solution into the glass and a potential formation of CSH could be responsible for inhibiting glass dissolution. In addition, Na and K concentrations were observed to decrease in a 0.5 μm layer near the edge of the specimens but then increase at the level of bulk glass with distance. This implies that the glass corrosion process is influenced by ion exchange involving alkalis ions such as Na^+, K^+, and hydrogen-containing species, which can potentially be replaced by Ca. In summary, these results suggest that corrosion modeling of nuclear waste glasses should incorporate multiple elements to adequately account for environmental effects, such as co-location with cementitious-based materials or waste grouts. The eventual implementation of the co-disposed lysimeter test configuration at Hanford [33] will serve as an ideal test case for these modeling assumptions. Longer-term studies of glass corrosion in these test environments, including the GC solution, pH adjusted buffers, and sediment contacted solutions, are planned to examine the behavior of Ca and other elements in glass corrosion over extended timeframes.

5.0 Conclusions

The dissolution of borosilicate glass in various alkaline solutions including GC, pH 12 buffer adjusted, and pH 12 buffer solutions amended with Ca and other elements, was evaluated via PCT and SPFT experiments. The GC and Ca-amended leach solutions showed lower dissolution rates, alteration layer thickness, and surface area of the corroded glass compared to solutions at the same pH with and without amendments with Si and Al. SEM analyses indicated the formation of precipitates with rhombohedral morphology on the glass surface in the GC and Ca-amended solutions that were associated with Ca enrichment on the glass surface. This observation may have arisen from the precipitation of either calcium borate or calcium silicate hydrates and the formation

of calcium carbonate, saturated from GC solution. These results suggest that, despite the expected trend of higher glass dissolution rates resulting from exposure to high alkaline solution, the presence of dissolved Ca (in conjunction with Si and Al) slows the dissolution of the glass. In a proposed lysimeter test configuration at Hanford where infiltrating water would contact a grout before the glass, the dissolution of the glass may, in fact, slow below predicted values that only consider the effect of increased pH. Further work is ongoing to expand this effect to leachates that have contacted disposal sediments to better replicate disposal environments and assess the extent of this observed effect.

Declaration of interests: The authors declare that they have no known competing financial interests or personal relationships that could have appeared to influence the work reported in this paper.

Acknowledgment

This research was supported by the U.S. Department of Energy's Office of Environmental Management under Cooperative Agreement #DE-EM0000598 (PI Dr. Leonel Lagos). The field lysimeter test discussed in this paper is funded by Washington River Protection Solutions, LLC and operated by Pacific Northwest National Laboratory.

References:

1. Ojovan, M. I.; Lee, W. E., Glassy wasteforms for nuclear waste immobilization. *Metallurgical and Materials Transactions A* **2011,** *42* (4), 837-851.
2. Grambow, B., Nuclear waste glasses-How durable? *Elements* **2006,** *2* (6), 357-364.
3. Gin, S.; Abdelouas, A.; Criscenti, L. J.; Ebert, W. L.; Ferrand, K.; Geisler, T.; Harrison, M. T.; Inagaki, Y.; Mitsui, S.; Mueller, K. T., An international initiative on long-term behavior of high-level nuclear waste glass. *Materials Today* **2013,** *16* (6), 243-248.
4. Vienna, J. D.; Ryan, J. V.; Gin, S.; Inagaki, Y., Current understanding and remaining challenges in modeling long-term degradation of borosilicate nuclear waste glasses. *International Journal of Applied Glass Science* **2013,** *4* (4), 283-294.
5. Jantzen, C. M.; Brown, K. G.; Pickett, J. B., Durable glass for thousands of years. *International Journal of Applied Glass Science* **2010,** *1* (1), 38-62.
6. Ribet, S.; Gin, S., Role of neoformed phases on the mechanisms controlling the resumption of SON68 glass alteration in alkaline media. *Journal of Nuclear Materials* **2004,** *324* (2-3), 152-164.
7. Eyring, H., The activated complex in chemical reactions. *The Journal of Chemical Physics* **1935,** *3* (2), 107-115.

8. McGrail, B.; Ebert, W.; Bakel, A.; Peeler, D., Measurement of kinetic rate law parameters on a Na- Ca- Al borosilicate glass for low-activity waste. *Journal of Nuclear Materials* **1997,** *249* (2-3), 175-189.
9. Nagy, K., Dissolution and precipitation kinetics of sheet silicates. *Chemical weathering rates of silicate minerals* **2018**, 173-234.
10. Pierce, E. M.; Rodriguez, E. A.; Calligan, L. J.; Shaw, W. J.; McGrail, B. P., An experimental study of the dissolution rates of simulated aluminoborosilicate waste glasses as a function of pH and temperature under dilute conditions. *Applied Geochemistry* **2008,** *23* (9), 2559-2573.
11. Freedman, V. L.; Ryan, J. V.; Bacon, D. H. *Immobilized Low-Activity Waste Glass Release Data Package for the Integrated Disposal Facility Performance Assessment*; Pacific Northwest National Lab.(PNNL), Richland, WA (United States): 2015.
12. Neeway, J. J.; Rieke, P. C.; Parruzot, B. P.; Ryan, J. V.; Asmussen, R. M., The dissolution behavior of borosilicate glasses in far-from equilibrium conditions. *Geochimica et Cosmochimica Acta* **2018,** *226*, 132-148.
13. Cailleteau, C.; Devreux, F. o.; Spalla, O.; Angeli, F.; Gin, S., Why do certain glasses with a high dissolution rate undergo a low degree of corrosion? *The Journal of Physical Chemistry C* **2011,** *115* (13), 5846-5855.
14. Cailleteau, C.; Angeli, F.; Devreux, F.; Gin, S.; Jestin, J.; Jollivet, P.; Spalla, O., Insight into silicate-glass corrosion mechanisms. *Nature materials* **2008,** *7* (12), 978-983.
15. Icenhower, J. P.; Samson, S.; Lüttge, A.; McGrail, B. P., Towards a consistent rate law: glass corrosion kinetics near saturation. *Geological Society, London, Special Publications* **2004,** *236* (1), 579-594.
16. Crum, J. V.; Reiser, J. T.; Parruzot, B. P.; Neeway, J. J.; Bonnett, J. F.; Kerisit, S. N.; Cooley, S. K.; Ryan, J. V.; Smith, G. L.; Asmussen, R. M., Seeded Stage III glass dissolution behavior of a statistically designed glass matrix. *Journal of the American Ceramic Society* **2021,** *104* (8), 4145-4162.
17. Utton, C.; Hand, R.; Bingham, P.; Hyatt, N.; Swanton, S.; Williams, S., Dissolution of vitrified wastes in a high-pH calcium-rich solution. *Journal of nuclear materials* **2013,** *435* (1-3), 112-122.
18. Kaspar, T. C.; Reiser, J. T.; Ryan, J. V.; Wall, N. A., Non-destructive characterization of corroded glass surfaces by spectroscopic ellipsometry. *Journal of Non-Crystalline Solids* **2018,** *481*, 260-266.
19. Vernaz, E.; Gin, S.; Jégou, C.; Ribet, I., Present understanding of R7T7 glass alteration kinetics and their impact on long-term behavior modeling. *Journal of Nuclear Materials* **2001,** *298* (1-2), 27-36.
20. National Academies of Sciences, E.; Medicine, Final Review of the Study on Supplemental Treatment Approaches of Low-Activity Waste at the Hanford Nuclear Reservation: Review# 4. **2020**.
21. Paul, A., *Chemistry of glasses*. Springer Science & Business Media: 1989.
22. Sjöberg, S., Silica in aqueous environments. *Journal of Non-Crystalline Solids* **1996,** *196*, 51-57.
23. Okhrimenko, D.; Nielsen, C.; Lakshtanov, L.; Dalby, K.; Johansson, D.; Solvang, M.; Deubener, J.; Stipp, S., Surface Reactivity and Dissolution Properties of Alumina–Silica Glasses and Fibers. *ACS applied materials & interfaces* **2020,** *12* (32), 36740-36754.
24. Jégou, C.; Gin, S.; Larché, F., Alteration kinetics of a simplified nuclear glass in an aqueous medium: effects of solution chemistry and of protective gel properties on diminishing the alteration rate. *Journal of Nuclear Materials* **2000,** *280* (2), 216-229.
25. Gin, S., Protective effect of the alteration gel: a key mechanism in the long-term behaviour of nuclear waste glass. **2001**.
26. Frugier, P.; Chave, T.; Gin, S.; Lartigue, J.-E., Application of the GRAAL model to leaching experiments with SON68 nuclear glass in initially pure water. *Journal of Nuclear Materials* **2009,** *392* (3), 552-567.
27. Chave, T.; Frugier, P.; Gin, S.; Ayral, A., Glass–water interphase reactivity with calcium rich solutions. *Geochimica et Cosmochimica Acta* **2011,** *75* (15), 4125-4139.

28. Backhouse, D. J.; Fisher, A. J.; Neeway, J. J.; Corkhill, C. L.; Hyatt, N. C.; Hand, R. J., Corrosion of the International Simple Glass under acidic to hyperalkaline conditions. *npj Materials Degradation* **2018,** *2* (1), 1-10.
29. Maraghechi, H.; Rajabipour, F.; Pantano, C. G.; Burgos, W. D., Effect of calcium on dissolution and precipitation reactions of amorphous silica at high alkalinity. *Cement and Concrete Research* **2016,** *87*, 1-13.
30. Nicoleau, L.; Nonat, A.; Perrey, D., The di-and tricalcium silicate dissolutions. *Cement and Concrete Research* **2013,** *47*, 14-30.
31. Neeway, J. J.; Emerson, H. P.; Asmussen, R. M.; Yamagata, A. L. F.; Meyer, P. D., Review of intermediate-scale field tests in support of disposal of waste forms. *Chemosphere* **2023**, 140625.
32. Rogers, R. D.; McConnell Jr, J. *Lysimeter literature review*; US Nuclear Regulatory Commission (NRC), Washington, DC (United States). Div. of Regulatory Applications; EG and G Idaho, Inc., Idaho Falls, ID (United States): 1993.
33. Bacon, D. H.; Meyer, P. D.; Neeway, J. J.; Fang, Y.; Asmussen, R. M.; Strickland, C. E. *Field-Scale Lysimeter Studies of Low-Activity Waste Form Degradation*; Pacific Northwest National Lab.(PNNL), Richland, WA (United States): 2018.
34. Meyer, P. D.; Asmussen, R. M.; Neeway, J. J.; Thomle, J. N.; Ekre, R.; Bacon, D. H.; Smith, G. L.; Mabrouki, R. B.; Swanberg, D. J. In *Field-Scale Lysimeter Studies of Glass and Cementitious Waste Forms at the Hanford Site-20392*, WM Symposia, Inc., PO Box 27646, 85285-7646 Tempe, AZ (United States): 2020.
35. Esh, D., Pinkston,K., Yadav, P., Parks, L., M. Heath *Draft Waste Incidental to Reprocessing Evaluation for Vitrified Low-Activity Waste Disposed Onsite at the Hanford Site, Washington*; U.S. Nuclear Regulatory Commission Office of Nuclear Material Safety and Safeguards Washington, DC 20555-0001: 2022.
36. Muller, I. S.; Viragh, C.; Gilbo, K.; Pegg, I. L.; Skeen, R. S. *ILAW Glass Ion-Exchange Rate Testing (Final Report FY2020)*; Washington River Protection Solutions, Richland, WA (United States); The Catholic Univ. of America, Washington, DC (United States); USDOE Office of River Protection (ORP), Richland, WA (United States): 2020.
37. Neeway, J. J.; Asmussen, R. M.; Cordova, E. A.; Lonergan, C. E.; Williams, B. D.; Leavy, I. I.; Mcelroy, E. M. *FY2017 ILAW Glass Corrosion Testing with the Single-Pass Flow-Through Method*; Pacific Northwest National Lab.(PNNL), Richland, WA (United States): 2018.
38. D1193–06, A., Standard specification for reagent water. ASTM International, West Conshohocken, PA, 2018

39. C1285-21, Standard Test Methods for Determining Chemical Durability of Nuclear, Hazardous, and Mixed Waste Glasses and Multiphase Glass Ceramics: The Product Consistency Test (PCT). In *ASTM International, West conshohocken, PA*, 2021.
40. C1662-18, Standard Practice for Measurement of the Glass Dissolution Rate Using the Single-Pass Flow-Through Test Method. In *ASTM International, West Conshohocken, PA*, 2018.
41. Icenhower, J. P.; Strachan, D. M.; McGrail, B. P.; Scheele, R. D.; Rodriguez, E. A.; Steele, J. L.; Legore, V. L., Dissolution kinetics of pyrochlore ceramics for the disposition of plutonium. *American Mineralogist* **2006,** *91* (1), 39-53.
42. Wellman, D. M.; Icenhower, J. P.; Weber, W. J., Elemental dissolution study of Pu-bearing borosilicate glasses. *Journal of Nuclear Materials* **2005,** *340* (2-3), 149-162.
43. Gudavalli, R. K.; Katsenovich, Y. P.; Wellman, D. M.; Idarraga, M.; Lagos, L. E.; Tansel, B., Comparison of the kinetic rate law parameters for the dissolution of natural and synthetic autunite in the presence of aqueous bicarbonate ions. *Chemical Geology* **2013,** *351*, 299-309.
44. Gudavalli, R.; Katsenovich, Y.; Wellman, D., Quantification of kinetic rate law parameters for the dissolution of natural autunite in the presence of aqueous bicarbonate ions at high concentrations. *Journal of environmental radioactivity* **2018,** *190*, 1-9.

45. Pierce, E. M.; Icenhower, J. P.; Serne, R. J.; Catalano, J. G., Experimental determination of UO2 (cr) dissolution kinetics: Effects of solution saturation state and pH. *Journal of Nuclear Materials* **2005,** *345* (2-3), 206-218.
46. Asmussen, R. M.; Pearce, C. I.; Miller, B. W.; Lawter, A. R.; Neeway, J. J.; Lukens, W. W.; Bowden, M. E.; Miller, M. A.; Buck, E. C.; Serne, R. J., Getters for improved technetium containment in cementitious waste forms. *Journal of hazardous materials* **2018,** *341*, 238-247.
47. Scheetz, B. E.; Freeborn, W. P.; Smith, D. K.; Anderson, C.; Zolensky, M.; White, W. B., The role of boron in monitoring the leaching of borosilicate glass waste forms. *MRS Online Proceedings Library (OPL)* **1984,** *44*, 129.
48. Gin, S.; Beaudoux, X.; Angéli, F.; Jégou, C.; Godon, N., Effect of composition on the short-term and long-term dissolution rates of ten borosilicate glasses of increasing complexity from 3 to 30 oxides. *Journal of Non-Crystalline Solids* **2012,** *358* (18-19), 2559-2570.
49. Arena, H.; Rébiscoul, D.; Podor, R.; Garcès, E.; Cabie, M.; Mestre, J.-P.; Godon, N., Impact of Fe, Mg and Ca elements on glass alteration: Interconnected processes. *Geochimica et Cosmochimica Acta* **2018,** *239*, 420-445.
50. Backhouse, D.; Corkhill, C.; Hyatt, N.; Hand, R., Investigation of the role of Mg and Ca in the structure and durability of aluminoborosilicate glass. *Journal of Non-Crystalline Solids* **2019,** *512*, 41-52.
51. Nellessen, M. A.; Gasda, P.; Crossey, L.; Peterson, E.; Ali, A.; Zhang, J.; Zhou, W.; Hao, M.; Spilde, M.; Newsom, H., Boron adsorption in clay minerals: Implications for martian groundwater chemistry and boron on Mars. *Icarus* **2023,** *401*, 115599.
52. Liu, M.; Guo, Q.; Luo, L.; He, T., Environmental impacts of geothermal waters with extremely high boron concentrations: Insight from a case study in Tibet, China. *Journal of Volcanology and Geothermal Research* **2020,** *397*, 106887.
53. Armelao, L.; Bassan, A.; Bertoncello, R.; Biscontin, G.; Daolio, S.; Glisenti, A., Silica glass interaction with calcium hydroxide: a surface chemistry approach. *Journal of Cultural heritage* **2000,** *1* (4), 375-384.
54. Atila, A.; Ouaskit, S.; Hasnaoui, A., Ionic self-diffusion and the glass transition anomaly in aluminosilicates. *Physical Chemistry Chemical Physics* **2020,** *22* (30), 17205-17212.
55. Mercado-Depierre, S.; Angeli, F.; Frizon, F.; Gin, S., Antagonist effects of calcium on borosilicate glass alteration. *Journal of nuclear materials* **2013,** *441* (1-3), 402-410.
56. Juilland, P.; Gallucci, E., Morpho-topological investigation of the mechanisms and kinetic regimes of alite dissolution. *Cement and Concrete Research* **2015,** *76*, 180-191.
57. Suzuki-Muresan, T.; Abdelouas, A.; Landesman, C.; Ait-Chaou, A.; El Mendili, Y.; Ribet, S.; Perrigaud, K.; Shitara, D.; Martin, C.; Bourbon, X., Alteration of vitrified intermediate level nuclear waste in alkaline media: effects of cementitious materials, pH and temperature. *RSC advances* **2018,** *8* (66), 37665-37680.
58. Erd, R., Supplement to Mellor's Comprehensive Treatise on Inorganic and Theoretical Chemistry. Longman, New York: 1980.
59. Nozawa, S.; Sato, T.; Otake, T., Effect of dissolved silica on immobilization of boron by magnesium oxide. *Minerals* **2018,** *8* (2), 76.
60. Schwieger, W.; Brunner, E., Isomorphous substitution of silicon by boron in layered sodium silicate hydrates. *Colloid and Polymer Science* **1992,** *270*, 935-938.
61. Gutzmer, J.; Beukes, N. J., Mineral paragenesis of the Kalahari managanese field, South Africa. *Ore Geology Reviews* **1996,** *11* (6), 405-428.
62. Pekov, I. V.; Zubkova, N. V.; Chukanov, N. V.; Yapaskurt, V. O.; Britvin, S. N.; Kasatkin, A. V.; Pushcharovsky, D. Y., Oyelite: new mineralogical data, crystal structure model and refined formula Ca5BSi4O13 (OH) 3· 4H2O. *European Journal of Mineralogy* **2019,** *31* (3), 595-608.
63. Damodaran, K.; Gin, S.; De Montgolfier, J.-V.; Jegou, C.; Delaye, J.-M., Behavior of B in passivating gels formed on International Simple Glass in acid and basic pH. *Journal of Non-Crystalline Solids* **2022,** *598*, 121938.

64. Mattigod, S. V.; Frampton, J. A.; Lim, C. H., Effect of ion-pair formation on boron adsorption by kaolinite. *Clays and Clay Minerals* **1985,** *33*, 433-437.
65. Chen, W.-T.; Ho, S.-B.; Lee, D.-Y., Effect of pH on boron adsorption-desorption hysteresis of soils. *Soil science* **2009,** *174* (6), 330-338.
66. Yang, W., *Solubilities of selected borosilicate minerals between 25 degrees and 250 degrees Celcius and P (V)= P (water)*. Washington State University: 1990.